Agricultural and Forest Meteorology 247 (2017) 385–398

Contents lists available at ScienceDirect

Agricultural and Forest Meteorology

journal homepage: www.elsevier.com/locate/agrformet

Research paper

Modeling the effects of management and elevation on West Texas dryland cotton production

Steven A. Mauget[a,*], Pradip Adhikari[b], Gary Leiker[a], R. Louis Baumhardt[c], Kelly R. Thorp[d], Srinivasulu Ale[e]

[a] U.S. Department of Agriculture-Agricultural Research Service USDA Plant Stress and Water Conservation Laboratory, Lubbock, TX 79415, United States
[b] Oklahoma State University, Stillwater, OK 74078, United States
[c] U.S. Department of Agriculture-Agricultural Research Service, USDA Conservation and Production Research Laboratory, Bushland, TX 79012, United States
[d] U.S. Department of Agriculture-Agricultural Research Service, Arid Land Agricultural Research Center, Maricopa, AZ 85138, United States
[e] Texas A & M AgriLife Research and Extension Center, Vernon, TX, 76385, United States

ARTICLE INFO

Keywords:
Regional crop modeling
DSSAT
Calibration
Regional frequency analysis
Yield risk

ABSTRACT

As the Ogallala Aquifer depletes there is a need to identify management options that might make un-irrigated cotton production sustainable over the U.S. Southern High Plains (SHP). To explore those options, the CSM-CROPGRO-Cotton model was used to simulate the effects of planting options and elevation effects on SHP dryland cotton production. Of the management variables that define the 56 planting options simulated, planting date and density account for the most variability in median SHP yields. Cooler SHP growing seasons have the effect of reducing median lint yields relative to those simulated over the lower elevations of the nearby Rolling Plains. This effect is not as evident in median Rolling Plains yields, which suggests it can be traced to the cooler growing environment of the higher SHP elevations. Also, at both higher and lower elevations lower planting densities maximize median yields, while higher densities result in the lowest yields. These results suggest that the yield suppressing effect of the SHP region's cooler growing conditions might be compensated for by planting early whenever possible and planting at lower densities. The clear decreasing effect on median yields at higher elevation also suggests the possibility of SHP cotton production moving to the lower elevations of the nearby Rolling Plains as Ogallala Aquifer levels drop.

1. Introduction[1]

During each year of 1965–2014 the state of Texas led the U.S. in both the planted acreage and production of upland cotton (ERS, 2016a). Within Texas the Southern High Plains (SHP) is a key production area, with the 10 highest producing counties in terms of acres harvested located in a growing region centered on the city of Lubbock (NASS 2016a). As cotton is the state's leading cash crop, with more than $2.0 Billion U.S in lint and seed sales in 2015 (NASS 2016b), cotton production is a central component of the West Texas economy.

But although it is a major cotton production area, in some respects the SHP environment is not ideally suited to growing cotton. Peng et al. (1989) and Morrow and Krieg (1990) cited the region's semi-arid and cool growing conditions and low levels of soil nitrogen and phosphorus as leading factors limiting production. Most importantly, the region's summer climate is water-limited relative to the needs of cotton. Median summer rainfall (29.2 cm) is slightly more than 1/3rd of median potential cotton crop evapotranspiration (84.6 cm) (Mauget et al., 2013). Because of this shortfall cotton crops are deficit irrigated where possible (Baumhardt et al., 2008), but in the coming decades a gradual shift to un-irrigated 'dryland' production is expected due to the ongoing depletion of the Ogallala Aquifer (McGuire 2007; Sophocleous 2010; Scanlon et al., 2012; Haacker et al., 2016).

In addition to being dry relative to the potential needs of cotton, the area's elevation also introduces temperature limitations. Fig. 1 maps the GTOPO30 elevation contours of West Texas (USGS 2015), and the locations of 32 weather stations maintained by the West Texas Mesonet (WTM: Schroeder et al., 2005). Between the relatively flat SHP growing region and the Rolling Plains to the east is an escarpment known locally as the West Texas Caprock. In Fig. 1 this feature roughly follows the 950 m elevation isoline. The rise in elevation between the two

* Corresponding author at: USDA-ARS Plant Stress and Water Conservation Laboratory, Lubbock, Texas, 3810 4th Street, Lubbock, Texas, 79415, United States.
E-mail address: Steven.Mauget@ars.usda.gov (S.A. Mauget).
[1] Southern High Plains (SHP); West Texas Mesonet (WTM); Decision Support System for Agrotechnology Transfer (DSSAT).

http://dx.doi.org/10.1016/j.agrformet.2017.07.009
Received 14 February 2017; Received in revised form 12 July 2017; Accepted 13 July 2017
Available online 06 October 2017
0168-1923/ Published by Elsevier B.V.

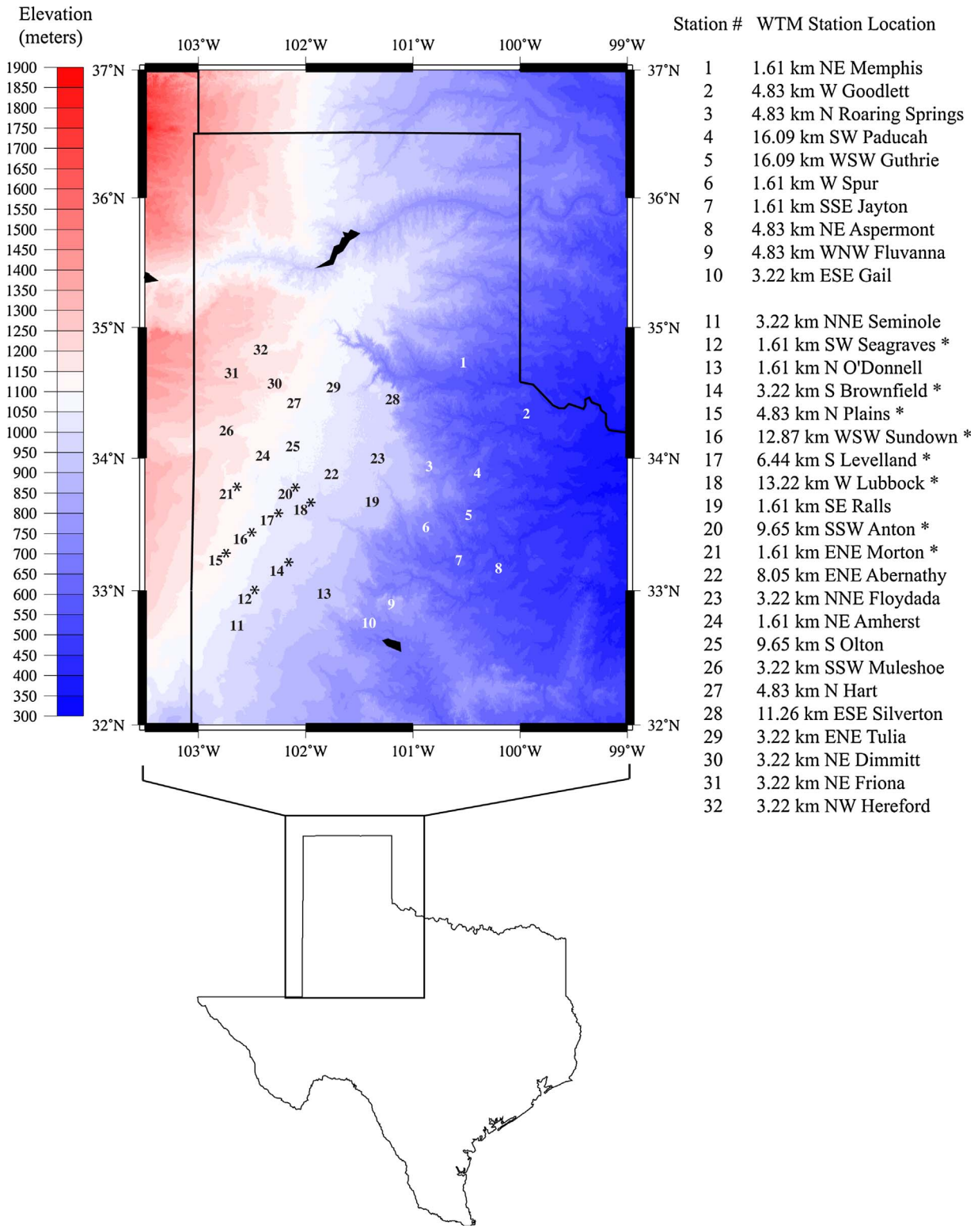

Fig. 1. Locations of the 32 West Texas Mesonet (WTM) stations used to provide daily CSM-CROPGRO-Cotton weather inputs. Stations 1–10 mark lower elevation station sites, while stations 11–32 mark sites over the higher elevation Southern High Plains cotton production region. Starred stations mark the high elevation stations used to provide weather inputs in the model calibration trials described in Section 4.2.

regions is about equal to the difference between the mean elevation of WTM stations 1–10 in Fig. 1 (659 m) and the remaining 22 SHP stations to the west above the Caprock (1069 m). Physical atmospheric processes, i.e., dry and wet adiabatic lapse rates, produce environmental cooling with increased elevation. Assuming the International Standard Atmosphere lapse rate of $-6.5\ ^{\circ}C\ km^{-1}$, the higher elevation stations would result in, on average, 2.7 °C fewer growing degree days (GDD)[2] per day when degree days are accumulated. Over a 154 day summer growing season (15 May–15 Oct.) with degree days accumulated on

[2] GDD represents the accumulation over time of daily average temperature above a 15.6 °C (60 °F) threshold.

each day, this daily average would translate into 410 °C fewer GDD at the higher elevations. This elevation-related decrease is approximately 30% of the range of summer GDD values (1400–1500 °C) that have been estimated to maximize SHP cotton lint yields (Peng et al., 1989).

Given an expected shift to dryland production with an accompanied effect on decreased yields and profits, there is a need to identify management strategies that might make such production sustainable in the SHP environment. But identifying the effects of management practices and elevation on agricultural yields through field trials is potentially time and resource intensive. Distinguishing management effects from those associated with the year-to-year variation in growing season climate requires conducting trials over multiple years. Exploring the effects of a range of management strategies would require repeating each year's trials over a similar range of replications. To estimate the potentially limiting effects of elevation on yield, those trials would have to be repeated at low and high elevation field sites.

An alternative approach would be to use a cotton crop model to simulate dryland production using weather records from high and low elevations. The modeling procedure used here is based on driving the Cropping System Model (CSM)-CROPGRO-Cotton model (Messina et al., 2004; Pathak et al., 2007, 2012) with daily weather data from Fig. 1's 32 WTM weather stations during 2005–2015. The use of calibrated crop models can allow for the generation of yield outcomes across an arbitrary but controlled range of initial conditions and management options. An additional advantage of the use of crop models is that they can be used to estimate the effects of projected or hypothetical environmental conditions. This approach has been commonly used to estimate the effects of global or regional climate change on agricultural production (Rosenzweig and Hillel 1993; Hillel and Rosenzweig 2011; Angulo et al., 2013 and references therein). Here, the CSM-CROPGRO-Cotton model is run with both un-modified and modified weather inputs to isolate the effects of elevation on SHP cotton yields.

An important feature of the modeling procedure followed here is the generation of distributions of yield outcomes. This approach is based on the fundamental principle of Regional Frequency Analysis (Hosking and Wallis 1997), which combines data from multiple weather or streamflow gage stations in climatically homogenous regions to provide better sampling of climate variability. Simulated yields derived from data from mesonet weather stations in a geographically limited growing region can provide improved sampling of precipitation-related yield effects, and better resolution of the probabilistic effects of management and environment. The resulting model-generated distributions can also be used as the basis of a framework for estimating climate-related risk and defining management practices that maximize yield. Mauget et al. (2009) proposed that producers might increase profits by adopting practices that are optimized to current climate, price, and cost conditions. An initial step for identifying those practices and estimating the associated risk is calculating the probabilities of yield outcomes given current climate conditions. Estimating those probabilities in turn requires yield ensembles that may be achievable only through a modeling approach. Here, the formation of these distributions is made possible by the use of high-quality weather inputs from the WTM's dense network of stations over 10 summer growing seasons.

In the following, Section 2 describes the daily WTM weather data used to drive the CSM-CROPGRO-Cotton model, while Section 3 provides a description of the SHP summer growing environment based on that data. Section 4 gives an overview of the DSSAT Cropping System Model, and a description of the approach used here to calibrate CSM-CROPGRO-Cotton for SHP dryland production. Section 5 describes the modeled effects of management and elevation on SHP lint yields. This section begins with an estimation of elevation's effect on median lint yield under production scenarios defined by 56 planting options and 3 initial soil moisture conditions. Then, the potential distributional effects associated with optimal planting options for the SHP region's high elevation conditions are described. Finally, this section estimates the potential yield limiting effects of elevation assuming those optimal planting options. Section 6 provides a discussion of the possible implications to current and future West Texas cotton production.

2. West Texas Mesonet data description and quality control

The daily weather data inputs used to drive the CSM-CROPGRO-Cotton model were derived from sub-daily data provided by West Texas Mesonet weather stations (Schroeder et al., 2005). Although the WTM currently consists of 92 stations, the 22 high elevation stations used here (stations 11–32) were selected based on their being mainly located within the major NASS District 12 Southern High Plains cotton growing region. Stations 1–10 were selected based on their location in the adjoining lower elevations of the Rolling Plains region. All stations were also required to provide continuous data, apart from minor data gaps, since 1 Jan. 2005. Each WTM station reports meteorological data; i.e., temperature, dew point temperature, precipitation, solar radiation, barometric pressure and wind speed, every 5 min. In addition, soil temperatures at 5, 10, and 20 cm, and estimates of soil water content at 5, 20, 60 and 75 cm are provided every 15 min. The daily WTM data used here for the 2005–2015 summer cropping seasons was derived from archived sub-daily data that was subjected to the quality control (QC) procedures described in Schroeder et al. (2005). The daily values calculated here include minimum (T_{min}) and maximum temperature (T_{max}) at 2.0 m, cumulative precipitation (P), solar radiation (R_S), daily mean dew point temperature (T_{dew}), 2.0 m wind speed (U_2), and daily soil temperature at 20 cm (ST_{20}). Outlier values in the daily data were tested for following the detection tests of Durre et al. (2010). When outlying values were detected, or when more than 80% of a variable's sub-daily measurements were found to be missing, the day's value was set to null. A missing data infill procedure substituted null daily precipitation values with values generated by a weather generator (Hanson et al., 1994), while null values for the remaining variables were replaced with values from the nearest WTM station that had passed the QC outlier tests.

As the meteorological basis of a regional crop modeling study, the use of WTM data provides two advantages. First, while most weather stations in the U.S. cooperative network measure only daily $T_{min,}$ T_{max}, and P, WTM stations report a more complete set of variables. The additional R_S,U_2, and T_{dew} variables eliminate the need to estimate weather inputs via parameterization or stochastic generation methods ditional R_S,U_2, and T_{dew} variables eliminate the need to estimate weather inputs via parameterization or stochastic generation methods (Allen et al., 1998; Elizondo et al., 1994), and reduce the potential modeling error resulting from these schemes. The WTM network's station density provides a second advantage of using mesonet data. As noted in the Introduction, crop modeling based on weather inputs from multiple weather stations can result in improved sampling of weather-related yield effects. This is particularly useful in simulating rain-fed production in a water-limited environment, where site-to-site variation in precipitation can produce related variation in yield. A dense network of stations also makes it possible to better detect elevation's effects on growing season climate conditions and the resulting agricultural yields. Although the duration of Fig. 1's station network is limited to 11 years, the number of stations makes it possible to aggregate climate or yield outcomes across sites. Thus during 2005–2015 the ten lower elevation stations could provide as many as 111 station-years of summer climate or cotton lint yield outcomes, while the 22 higher elevation stations could provide as many as 242.

3. The Southern High Plains summer growing environment

Fig. 2a is a scatterplot of summer growing season (15 May–15 Oct.) growing degree days vs. station elevation calculated at each of Fig. 1 WTM stations during 2005–2015. The white circles and triangles show the values for Fig. 1's 22 higher elevation stations (Stations 11–32), while the gray circles and triangles show the values for the 10 low

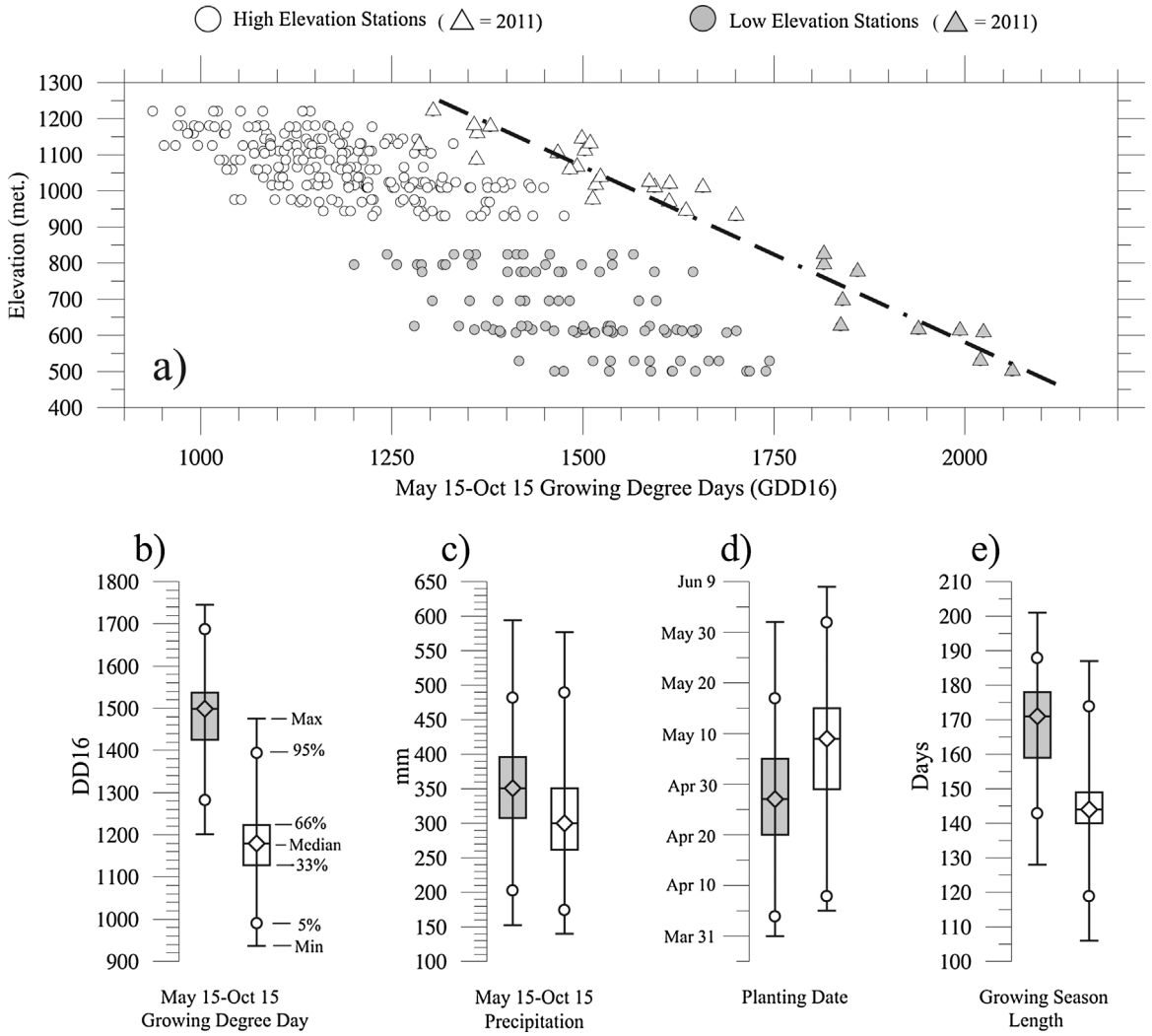

Fig. 2. a) Scatterplot of summer growing season (May 15–Oct. 15) growing degree days vs. elevation for each of Fig. 1's high and low elevation stations during 2005–2015. Triangles mark results for the summer of 2011. b) Bar and whisker diagrams showing the distribution of station-year summer growing degree days aggregated over Fig. 1's high (white bar) and low (gray bar) elevation stations during 2005–2010 and 2012–2015. c) As in (b) for summer growing season precipitation. d) As in (b) for the distribution of station-year planting dates defined by the end of the first 10 day spring period when mean 20 cm soil temperatures met or exceeded an 18.3 °C threshold. e) As in (b) for the distribution of growing season duration defined by the planting dates of (d) and harvest dates defined by the end of the same station-year's first 5 day fall period when GDD totals are less than 11.1 °C.

elevation stations (Stations 1–10). The effect of increasing elevation between the two groups of stations is seen in generally decreasing summer GDD values, although elevation effects are also evident within both groups of stations. The triangles show values for the summer of 2011, which was marked by extreme statewide drought in Texas (Hoerling et al., 2013). Fig. 2a's dashed line is a linear regression fit to the 2011 values, which indicates a decrease of 1028 °C summer degree days with each kilometer increase in elevation. When divided by the number of days over which these GDD totals were summed (154), this corresponds to a decrease of 6.67 °C km^{-1}, which is about equal to the International Standard Atmosphere lapse rate (−6.5 °C km^{-1}). Thus these elevation-related cooling effects are consistent with the physical tendency of the atmosphere to cool with increasing elevation. Given the extreme hot and dry conditions over West Texas during the summer of 2011, data from that outlier year was omitted in the formation of the WTM data distributions in Fig. 2b–e and was not used to model lint yields in the CSM-CROPGRO-Cotton calibration trials of Section 5, or the yield simulations described in Section 5.

The bar and whisker (BW) diagrams of Fig. 2b show the percentiles of the 220 summer GDD values for the 22 high elevation stations during 2005–2010 and 2012–2015, and the 100 values accumulated at the lower elevation stations during those 10 years. These BW diagrams mark the minimum, median (50th percentile), and maximum value, and the 5th, 33rd, 66th and 95th percentiles of GDD. As measured by the difference between the median of the low (1499 °C) and high (1180 °C) elevation distributions in Fig. 2b the difference in summer GDD between the two sets of stations is 319 °C, or ~78% of the 410 °C estimate made in Section 1 based on mean elevation and a standard atmospheric lapse rate. While the central tercile of the low elevation distribution, i.e. the range spanning the 33rd–66th percentile, falls within and above the 1400–1500 °C range estimated by Peng et al. (1989) to maximize lint yields, the same percentiles of the high elevation distribution fall well below that range. The counterpart distributions for May 15–Oct. 15 precipitation (Fig. 2c) shows a less pronounced tendency for wetter summer conditions at lower elevations, with the central tercile for the lower elevation stations displaced ~50 mm above the same percentiles of the higher elevation stations.

The soil temperature measurements reported by WTM stations make it possible to calculate the day of the year when temperatures are first suitable for planting. Boman and Lemon (2005) suggest that planting dates in the SHP region should occur at the end of the first 10 day period when mean 20 cm soil temperatures meet or exceed an 18.3 °C threshold. The Fig. 2d BW diagrams show the distribution of those dates for the 100 low elevation station-years and the 220 high elevation

station-years. Over the low elevation stations that date occurs as early as 31 March and as late as 1 June, with a median date of 27 April. Over the higher elevation sites cooler conditions generally delay planting under these guidelines, with corresponding dates of 5 April, 8 June, and 9 May. If a growing season's end date is defined as the final day of the first 5 day fall period when GDD totals are below 11.1 °C, then for each planting date in Fig. 2d the length of the subsequent growing season can be calculated. Fig. 2e shows the distributions of those values in days for both high and low elevation stations. Those BW diagrams show a clear shift towards shorter growing seasons at the higher elevations, with a median season length almost 4 weeks shorter than the lower elevation median. In summary, relative to nearby lower elevation stations, sites in the major SHP cotton growing region above the Caprock accrue fewer summer growing degree days, have delayed planting dates and shorter growing seasons, and have somewhat lower median summer rainfall totals.

4. The DSSAT cropping system model

The DSSAT Cropping System Model (Jones et al., 2003; Hoogenboom et al., 2012) is a modular set of integrated and standardized software components that simulates crop development over a single growing season, or sequences of growing seasons. A soil module defines soil characteristics on a layer-by-layer basis, calculates soil temperature, and simulates transport processes involving soil water, nitrogen (N), carbon, and residue. A weather module reads daily weather input files, and if necessary, estimates missing daily weather data using weather generators. A soil-plant-atmosphere (SPAM) module simulates soil evaporation, root water extraction, and plant transpiration. Various plant growth modules simulate the growth of specific crops. The module used here is CSM-CROPGRO-Cotton (Messina et al., 2004; Soler and Hoogenboom 2006; Pathak et al., 2007, 2012), which was developed based on a generic plant growth template module. A management operations module defines a cropping simulation's operational conditions, including planting and harvesting date, irrigation scheduling, and the application of fertilizer and residue. A more detailed summary of how CSM-CROPGRO-Cotton simulates crop development processes can be found in Thorp et al. (2014).

4.1. Modeled production conditions, planting options, and initial conditions

CSM-CROPGRO-Cotton simulations were conducted using the daily weather inputs from each of Fig. 1's WTM weather stations during 2005–2010 and 2012–2015, hereafter referred to as the 10 simulation years. To model the lint yield effects associated with a broad range of management practices, for each simulation year model runs were repeated under the planting options (PO) listed in Table 1. Thus for each station-year simulations were repeated under 56 options (PO1–PO56) defined by four planting densities, two N application rates, and seven planting dates. Table 1's planting densities approximate that of a locally conducted field study (Stapper and Fromme, 2011), and the simulations specified a row separation of 1.0 m. Nitrogen was applied at the rates of 30 and 60 kg ha^{-1}, with half of the application applied at planting and the remaining half applied in the simulations on 1 July. The seven planting dates were selected to evenly and approximately span the distribution of dates defined by Fig. 2d's high elevation BW diagram. The cultivar in all simulations was the Fibermax 9680B2RF variety, which was used in a recent study by Adhikari et al. (2016). The Fibermax cultivar's genetic and ecotype parameters in the simulations were those estimated by Adhikari et al. (2016), based on irrigated cotton field experiments conducted at the Texas A & M AgriLife Research Center at Halfway during 2010–2013 (Bordovsky and Mustian, 2013). Given the importance of soil water as an initial condition in dryland production, each station-year's simulation, for each management option, was in turn repeated under 3 initial soil moisture (ISM) conditions of 20%, 40%, and 60% of total available soil water capacity. Although there are a range of soil types across the SHP region, to control for the effects of soil type all the simulations were conducted with an Amarillo sandy loam (Fine-loamy, mixed, superactive, thermic Aridic Paleustalfs), one of four Great Plains soils evaluated in the lysimeter trials of Tolk and Howell (2010).

4.2. CSM-CROPGRO-Cotton calibration

For a SHP producer growing dryland cotton water is the most important variable that determines yields. As a result, a key requirement in modeling representative lint yields in this semi-arid environment is verifying the model's yield response to available soil water. In comparing observed and simulated seasonal crop evapotranspiration (ET_c) at the U.S. Arid Land Agricultural Research Center during 1990–2003, Thorp et al. (2014) found that cotton ET_c derived via the DSSAT-CSM's Priestley-Taylor and FAO-56 Penman-Monteith methods was underestimated by as much as 14% for the former method, and 16% for the latter. As an alternative approach Thorp et al. (2014) proposed and tested a single coefficient method of calculating potential crop ET (PET_c) based on ASCE standardized reference grass ET values (ET_o: Walter et al., 2005) and the LAI-based crop coefficient of DeJonge et al. (2012a,b). Here, a similar LAI-based dual coefficient potential evapotranspiration subroutine (PETACSE) was used (DeJonge and Thorp, 2017). This approach multiplies ASCE reference grass evapotranspiration by two coefficients that account for potential plant transpiration via a basal crop coefficient (K_{cb}) and potential surface evaporation via an evaporation coefficient (K_e).

$$PET_c = K_{CB}{*}\ ET_O + K_e{*}\ ET_O = PET_t + PET_e \quad (1)$$

Daily reference grass evapotranspiration is calculated using Eq. (1) of Walter et al. (2005),

$$ET_0 = \frac{0.408{*}\Delta{*}(R_n - G) + \gamma{*}(900/(T + 273)){*}U_2{*}(e_s - e_a)}{\Delta{+}\gamma(1 + 0.34U_2)} \quad (2)$$

where Δ is the slope of the saturation vapor pressure vs. temperature curve, R_n is the net daily surface radiation, G is the soil heat flux (set to 0.0 in PETASCE), γ is the psychometric constant, T is daily average temperature in °C, U_2 is the mean daily 2 m wind speed, and e_s and e_a are the daily saturation and actual water vapor pressure. The LAI-based basal crop coefficient is calculated via,

$$K_{cb} = K_{cmn} + (K_{cmx} - K_{cmn}){*}(1.0–\exp(-SK_c{*}LAI)) \quad (3)$$

where the K_{cmn} and K_{cmx} parameters define minimum and maximum K_{cb} values for limiting values of leaf area index (LAI), and SK_c is a shape parameter that defines the K_{cb} response to varying LAI. The calculation of K_e is used to quantify potential soil evaporation, but DSSAT-CSM routines are used to calculate actual soil evaporation. Actual plant transpiration in the DSSAT-CSM SPAM module is assigned as the minimum of the PET_t transpiration rate and the calculated potential total root water uptake (Jones et al., 2003; Boote et al., 2008). The model's total crop evapotranspiration is the sum of the actual plant transpiration and soil evaporation rates.

Two standards were used to calibrate the yield response of CSM-CROPGRO-Cotton as a function of the model's cumulative growing season ET_c under dryland SHP growing conditions. The first was the linear lint yield response functions derived from the lysimeter experiments of Tolk and Howell (2010) conducted in Bushland, Texas during 2005–2007. The second was the 2005–2015 mean of NASS Southern High Plains (District 12) annual un-irrigated lint yield averages (NASS 2016c). Like the modeled yields, this 2005–2015 average does not include the 2011 regional mean, which was not reported by NASS for that cropping year.

To reduce the time and computing resources required in the calibration trials, yields were modeled using daily weather data from eight WTM stations located in NASS District 12, which are marked in Fig. 1's

Table 1
Planting densities, nitrogen application rates, and planting dates defining the 56 planting options (PO) modeled in the CSM-CROPGRO-Cotton simulations.

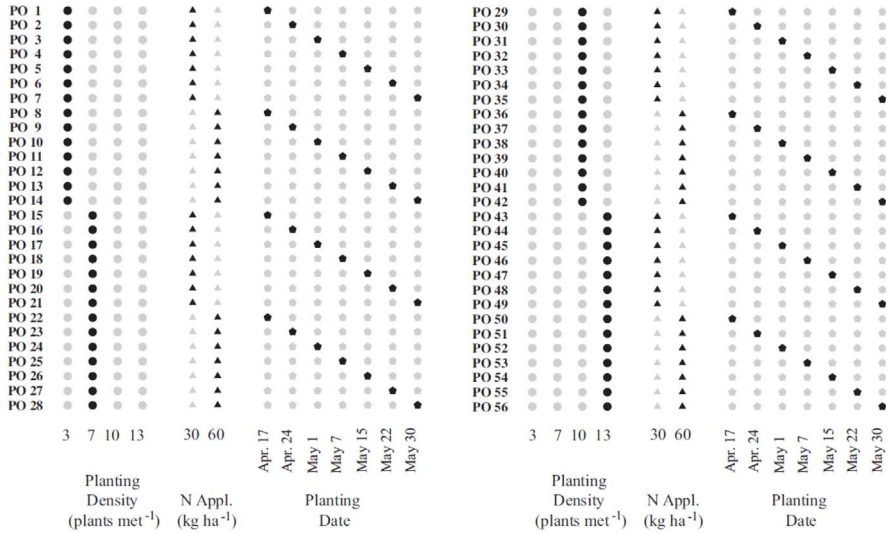

station location listing. These yields were modeled using a single mid-range management option (PO 25), but each station-year's model run was repeated under each of the 3 initial soil moisture conditions. Thus the calibration phase was based on model runs from 10 simulation years that produced 8*3*10 = 240 dryland seed cotton yields. Lint yields (Y_L) were estimated from the model's seed cotton yield output values based on the average seed to lint yield ratio (1.62) reported over the Economic Reporting Service's Prairie Gateway region in 2015 (ERS, 2016b). Calibration trials were conducted by modifying the contents of the $COGRO_{046}$·SPE and $COGRO_{046}$·CUL files to adjust evapotranspiration and cultivar parameters respectively. For each set of parameter conditions, the CSM-CROPGRO-Cotton executable was run in C shell scripts that generated the 240 seed cotton yields via repeated model runs in a UNIX command line environment.

Fig. 3a–d's blue and green lines mark the linear regressions of Y_L as a function of ET_c derived by Tolk and Howell (2010), hereafter TH10, for lysimeter field trials conducted with an Amarillo sandy loam soil in 2005 and 2007. The regression line for TH10 Amarillo soil trials conducted in 2006 are not used, as lint yields in that year's trials were not found to be significantly related to ET_c. The Fig. 3a scatterplot values mark the coordinates of the 240 simulated lint yields and seasonal ET_c values generated based on K_{cmn} (0.0), K_{cmx} (1.15) and SK_c (0.60) parameter values suggested by K. Thorp for Arizona irrigated cotton. The black, gray and white tokens indicate yields for the 20%, 40%, and 60% ISM levels, and the red line is the best-fit linear function for the 240 modeled calibration yields, i.e.,

$$Y_L = \beta 1 * ET_c + \beta_2 + \varepsilon \quad (4)$$

The calibration trial's goals were to achieve a modeled linear lint yield response similar to that of the 2005 and 2007 TH10 field trials (Table 2), and to reproduce the NASS 2005–2015 District 12 mean lint yield. In Fig. 3a the β_1 linear regression slope based on the Arizona cotton ET parameters (0.19) falls below that of the TH10 trials, and the average of the calibration yields (335 kg ha^{-1}) is 75% of the NASS District 12 average (447 kg ha^{-1}). Given the generally lower LAI of dryland SHP cotton relative to that of irrigated Arizona cotton, subsequent trials were carried out with lower SK_c values. These trials also used a lower K_{cmx} value (1.10) for High Plains cotton that is equal to a maximum mid-season value estimated via lysimeter field trials (Howell et al., 2004). Reducing SK_c has the effect of increasing lint yield per unit of evapotranspiration, i.e., β_1, and trials that gradually reduced the parameter's value to 0.5 (Fig. 3b) increased the mean β_1 yield response to ET_c to 0.23 and the mean lint yield to 415 kg ha^{-1}. As SK_c = 0.5 is the minimum value recommended by DeJonge et al. (2012a) for corn, attention turned to the adjustment of cultivar parameters.

Given their influence on yield output and photosynthesis rate, three cultivar parameters were adjusted from the values calculated by Adhikari et al. (2016): the maximum leaf photosynthesis rate (LFMAX), the maximum percentage of daily growth that is partitioned to seed plus shell (XFRT), and the threshing percentage (THRSH). The initial LFMAX value (1.10 mg CO_2 met^{-2} sec^{-1}) assumed an atmospheric CO_2 concentration of 350 parts per million (ppm). As current global levels exceed 400 ppm, LFMAX was increased to 1.18 based on the function relating CO_2 concentrations to cotton canopy photosynthesis rates estimated by Reddy et al. (2008). This adjustment resulted in a modest increase in mean yield to 425 kg ha^{-1} (Fig. 3c) and no change in the β_1 regression slope (Table 2). Increasing XFRT from 0.80 to 0.83 and THRSH from 70.0 to 72.0 resulted in a mean yield value (444 kg ha^{-1}) slightly below that of the NASS District 12 mean, but only a minor increase in the β_1 slope coefficient to 0.24 (Fig. 3d, Table 2). Further increases in XFRT and THRSH resulted in mean yields above the NASS mean, but no increase in the β_1 coefficient above 0.24. This reduced lint yield effect per unit of evapotranspiration relative to the field trial values (0.29, 0.31) suggests that the model may produce less lint for a fixed ET_c level relative to that measured in the TH10 field trials. However, this difference in yield response may be due to the difference in the production conditions in the lysimeter field trials and the model simulations. Of the 24 TH10 Amarillo soil replications during the 2005 and 2007 growing seasons, 9 were irrigated at levels sufficient to replace 100% of crop evapotranspiration. Another 9 were irrigated at 50% deficit levels, and the remaining 6 were irrigated at 25% levels or un-irrigated. By contrast, all of the modeled yield outcomes in the calibration trials simulated dryland production conditions, and one-third of those were initialized at low (20%) initial soil moisture conditions. As a result, Fig. 3d's weaker modeled yield response may be due to the higher proportion of simulated yield outcomes produced under low water conditions.

5. Management and elevation effects on Southern High Plains lint yields

Under each of the three ISM conditions, lint yields were simulated using Fig. 3d parameter values listed in Table 2 under each of Table 1's 56 planting options (PO). For each of the 168 ISM-PO combinations simulations were repeated using each WTM site's weather inputs during the ten simulation years. Then, the yields for each station-year were

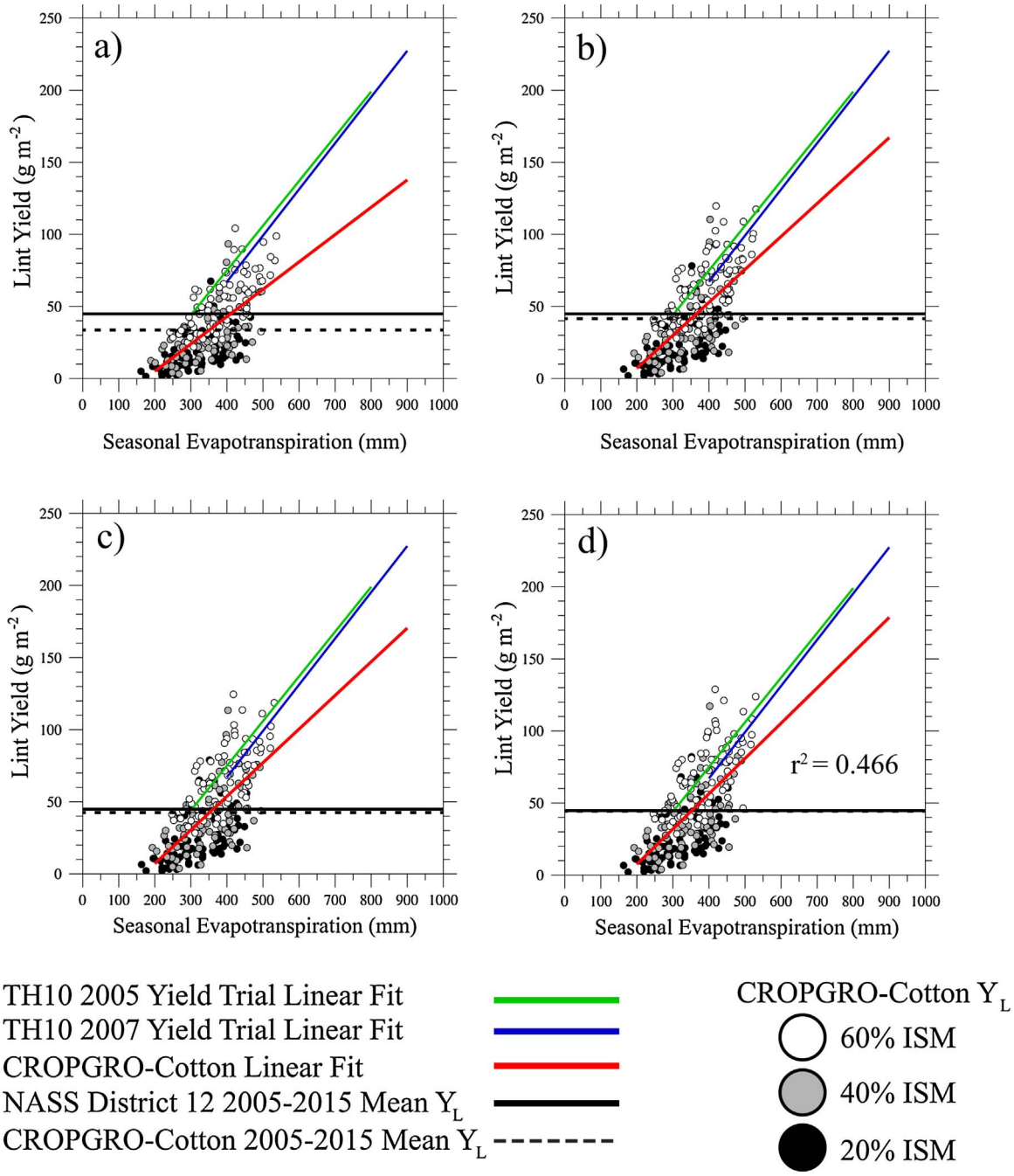

Fig. 3. a) Scatterplot of CSM-CROPGRO-Cotton lint yield vs. seasonal evapotranspiration values generated with weather inputs from eight SHP mesonet stations over ten simulation years. Black, gray, and white tokens show yields generated based on 20%–40%–60% initial soil water conditions. The linear regression lines for modeled and lysimeter field trial yields are marked as in the legend. The calibration trial's mean lint yield, linear regression parameters, and evapotranspiration and cultivar parameters are listed in Table 2. b) As in (a) for the 3b entries in Table 2. c) As in (a) for the 3c entries in Table 2. d) As in (a) for the 3d entries in Table 2. The r^2 value indicates the percentage of yield variance explained by the red CROPGRO-Cotton linear fit line.

Table 2
Mean lint yields in kg ha^{-1} ($\overline{Y}_L$), Eq. (4) regression parameters (β_1, β_2), Eq. (3) basal crop coefficient parameters (SK_c, K_{cmn}, K_{cmx}), and cultivar coefficients (XFRT, THRSH, LFMAX) for Fig. 3a–d calibration trials. TH2010 entries list Eq. (4) regression parameters for the Tolk and Howell (2010) lysimeter field trials during 2005 and 2007.

	$\overline{Y}_L$	β1	β2	SKc	Kcmn	Kcmx	XFRT	THRSH	LFMAX
Fig. 3a	0.19	−32.9	0.6	0	1.15	0.8	0.7	1.1	1.1
Fig. 3b	415	0.23	−38.7	0.5	0	1.1	0.8	0.7	1.1
Fig. 3c	425	0.23	−39.5	0.5	0	1.1	0.8	0.7	1.18
Fig. 3d	444	0.24	−41.4	0.5	0	1.1	0.83	0.72	1.18
TH2010(2005)	NA	0.31	−49	–	–	–	–	–	–
TH2010(2007)	NA	0.35	−33.8	–	–	–	–	–	–

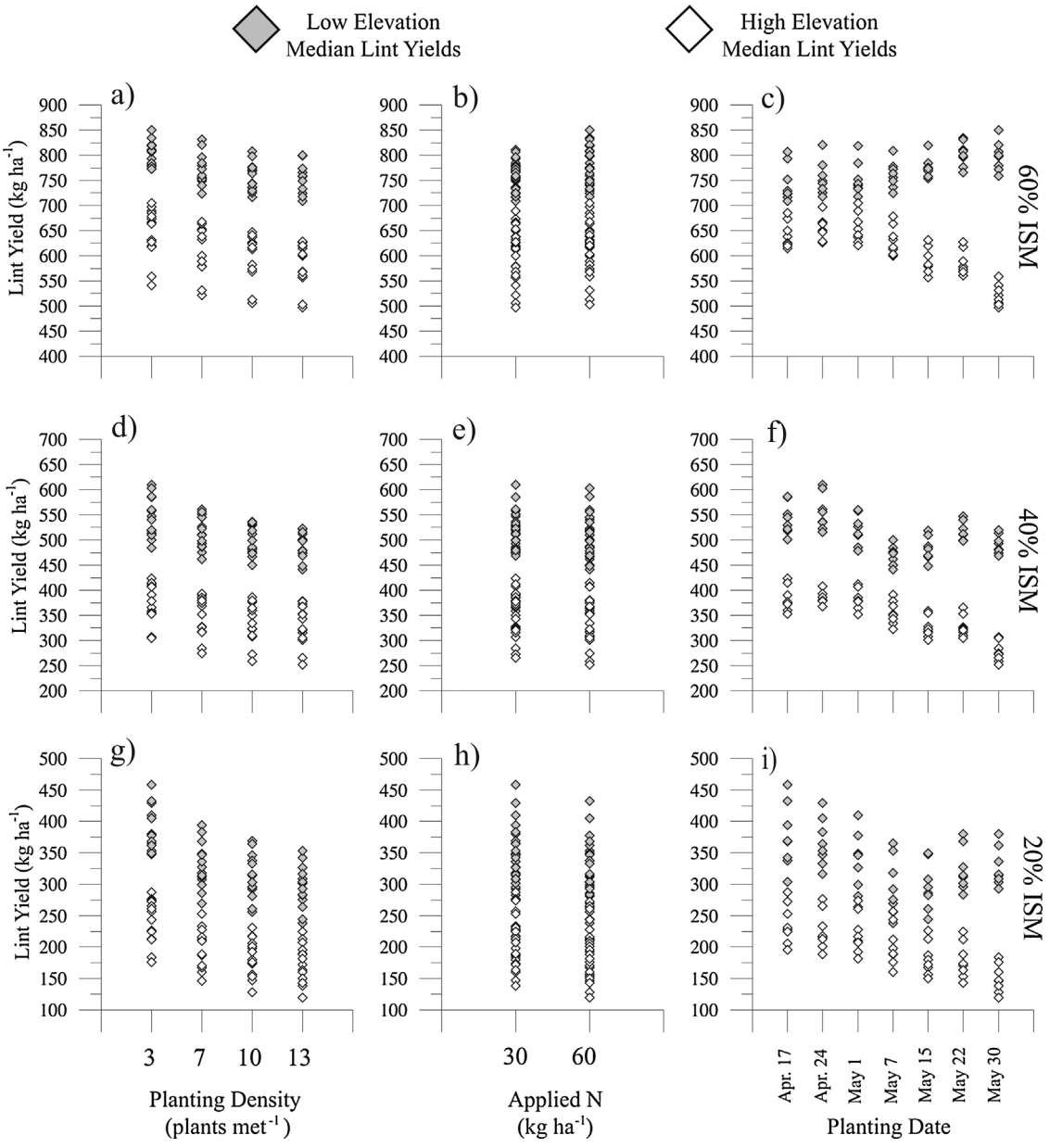

Fig. 4. a) Median lint yields resulting from Table 1's 56 planting options under 60% ISM conditions grouped by planting density. White (gray) diamonds mark medians of yield distributions derived from high (low) elevation weather station inputs. b) As in (a) with the median yields arranged by applied nitrogen rate. c) As in (a) with the median yields arranged by planting date. d) As in (a) for 40% ISM conditions. e) As in (b) for 40% ISM conditions. f) As in (c) for 40% ISM conditions. g) As in (a) for 20% ISM conditions. h) As in (b) for 20% ISM conditions. i) As in (c) for 20% ISM conditions.

aggregated over Fig. 1's high (stations 11–32) and low elevation (stations 1–10) WTM sites to form distributions of yield outcomes for each ISM-PO condition under both high and low elevation growing conditions. The number of yields in the resulting distributions are potentially equal to the total number of station-years resulting from both sets of stations, i.e., 220 yields for the high elevation stations, and 100 yields for the low elevation stations. As planting options with 17 Apr. planting dates were found to lead to simulated early crop failures at high elevations due to cool spring planting conditions, only the modeled yields from completed growing seasons were included in these distributions. As a result the number of yields in the high elevation distributions were less than 220 in 26 of the 168 ISM-PO conditions, but these yield counts never fell below 197. At the lower elevation all ISM-PO conditions produced yield distributions with 100 yields. These yield counts allow for calculating yield percentiles and describing these distributions using BW diagrams similar to that in Fig. 2b.

5.1. Median lint yield effects

Fig. 4a–c show the median yields of the high and low elevation distributions under the 60% ISM condition. Fig. 4a's white and gray diamonds show the 56 median lint yields for the high and low elevation stations grouped by the 4 planting densities. Fig. 4b shows the same median values grouped by the 2 N application levels, while Fig. 4c shows those values grouped according to the 7 planting dates. Fig. 4d–f show the effects of planting density, applied N, and planting date on median yield under the 40% ISM condition, while Fig. 4g–i show the same effects under the 20% ISM condition.

When sorted by planting density, Fig. 4a, d, and g show that high elevation median yields are uniformly lower than those resulting from the same ISM-PO condition simulated over the lower elevation stations. Apart from this clear elevation effect on yield, these figures also show more subtle planting date yield effects at the lowest and highest ISM

levels, a positive N effect at the highest ISM level, and relatively clear planting date effects on higher elevation yields. In Fig. 4a, d, and g, the highest median yields occur at the lowest planting density under all three ISM conditions, and there is a fairly clear tendency for median yields to decrease with increasing planting density. This tendency is particularly obvious at the lowest ISM level (Fig. 4g). At the highest ISM level the higher N application produces the highest median yield at both high and low elevations (Fig. 4b), but at the 20% ISM level (Fig. 4h) the lower N application produces the highest median yields at both elevations. Under each ISM condition in Fig. 4c, f and i high elevation median yields peak with either a 17 Apr. or 1 May planting, with planting dates after 1 May showing a uniform tendency for decreased yields as planting is delayed. At low elevations delayed planting tends to produce higher median yields under the 60% initial soil moisture conditions (Fig. 4c), but the highest median yields occur with earlier 17 Apr. or 24 Apr. planting dates at the 40% and 20% levels (Fig. 4f, i). However, unlike higher elevation median yields, the low elevation median yields of Fig. 4f and i show a less clear planting date effect than found at the higher elevation under the 40% and 20% ISM conditions.

5.2. The effects of optimal planting options at high elevation

Fig. 5 shows the BW diagrams for the planting options producing Fig. 4's highest (Fig. 5a, c, and e) and lowest (Fig. 5b, d, and f) median lint yields for each ISM level in the high elevation simulations. As in Fig. 4c, f, and i, planting on 17 Apr. or 1 May produces the highest median yields. At each ISM level the latest planting date (30 May) produces the lowest median yield. At the highest ISM level (Fig. 5a,b) the highest median yield is produced at the higher N application rate, and the lowest median at the lower rate. Conversely, at the 40% and 20% ISM levels the highest median yields result from the lower N application rate. The general pattern of higher yields with lower planting densities seen in Fig. 4a, d and g is also found in the maximum and minimum median outcomes in the 60% ISM simulations (Fig. 5a, b), 40% ISM simulations (Fig. 5c, d) and the 20% ISM simulations (Fig. 5e, f).

Each of Fig. 5a–f BW diagrams represent the distribution of as many as 220 station-years of yield simulations for one planting option. As a result, the lint yields from two planting options derived from the same station-year's weather inputs can be compared to calculate a yield effect (Δ_Y) resulting from choosing between those options. Thus under the 60% ISM condition, for example, the 2005 yields for Olton (Station 25) resulting from Fig. 5b's PO 49 simulation can be subtracted from the 2005 Olton yield resulting from Fig. 5a's PO 10 simulation to estimate the associated yield effect. Repeating this comparison for all 22 high elevation stations for each of the 10 simulation years produces a yield effect distribution with between 197 and 220 Δ_Y values. Fig. 5g's BW diagram shows the distribution of those yield effects, while Fig. 5h shows the Δ_Y distribution resulting from subtracting Fig. 5d yields from Fig. 5c yields under the 40% ISM condition. Fig. 5i shows the

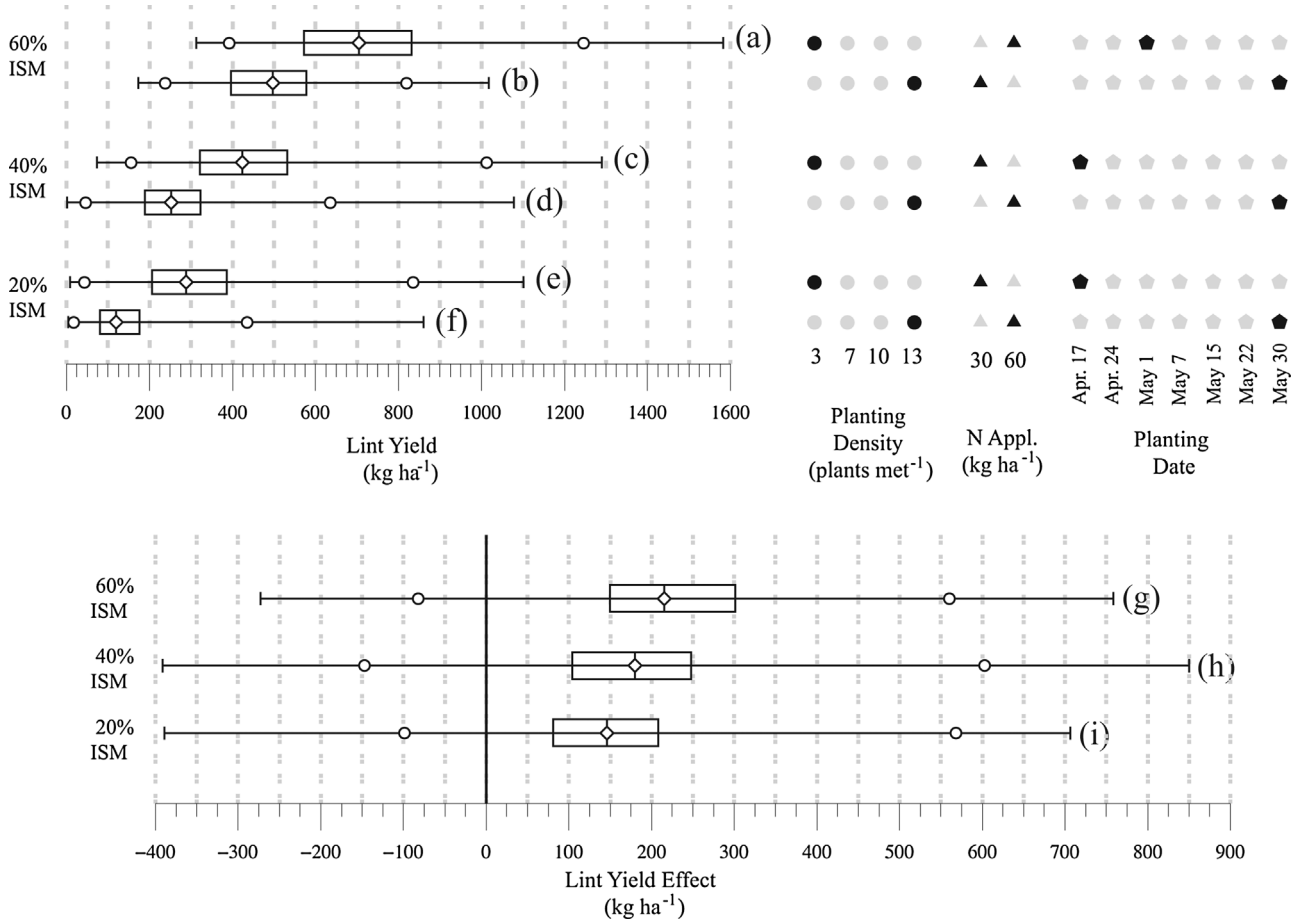

Fig. 5. a) Percentiles of high elevation lint yields for the planting option producing the highest median (PO 10) under 60% ISM conditions. Bar and whisker yield percentiles are as marked in Fig. 2b. b) As in (a) for the planting option producing the lowest median (PO 49) under 60% ISM conditions. c) As in (a) for the management option producing the highest median (PO 1) under 40% ISM conditions. d) As in (a) for the planting option producing the lowest median (PO 56) under 40% ISM conditions. e) As in (a) for the planting option producing the highest median (PO 1) under 20% ISM conditions. f) As in (a) for the planting option producing the lowest median (PO 56) under 20% ISM conditions. g) Percentiles of yield effects resulting from subtracting the PO 49 yields of (b) from the corresponding station-year's PO 10 generated yield in (a). h) Percentiles of yield effects resulting from subtracting the PO 56 yields of (d) from the corresponding station-year's PO 1 generated yield in (c). i) Percentiles of yield effects resulting from subtracting the PO 56 yields of (f) from the corresponding station-year's PO 1 generated yield in (e).

distribution of yield effects that result from subtracting Fig. 5f yields from Fig. 5e yields under the 20% ISM condition.

Because Fig. 5a–f show the yield distributions with the smallest and largest median yield values under each ISM condition, the corresponding Δ_Y distributions in Fig. 5g–i estimate 'Best minus Worst' yield effects resulting from the choice of the planting option producing the highest median yield. The percentiles of these distributions also allow for estimating the probability of those yield effects given recent summer growing season climate conditions over the SHP region. Thus under the 60% ISM condition, Fig. 5g's BW diagram indicates an 88% chance of a positive yield effect, and a 50% probability of a potential yield increase of 216 kg ha^{-1} or more. The number of samples in these distributions also allows for estimates of the probability of outcomes – positive and negative – in the tails of the distributions. For example, Fig. 5g indicates that, given the optimal MO 10 management option with high initial soil moisture, there is a 5% chance of a negative yield effect that might range between −82 and −273 kg ha^{-1}, and a 5% chance of a positive effect that could range between 560 and 758 kg ha^{-1}.

5.3. Distributional effects of elevation on lint yield

To estimate the effects of elevation (Z) on lint yield under Fig. 5's optimal high altitude management options (MO 10, MO 1, MO 1), Fig. 6 shows yield percentiles simulated using both high and low elevation weather inputs under those options and the three ISM conditions. Fig. 6a, c, and e reproduces the high elevation yield percentiles of Fig. 5a, c, and e, while Fig. 6b, d, and f mark the percentiles derived using the same ISM-PO conditions, but simulated based on the 100 station-years of weather inputs from Fig. 1's lower elevation stations.

In Fig. 6b, d, and f the lower elevation yield percentiles exceed the corresponding high elevation percentiles with two exceptions – the maximum yields under the 40% and 60% ISM condition. Under the 60% ISM condition (Fig. 6a, b) median yields are increased by 115 kg ha^{-1}, while the 40% (Fig. 6c, d) and 20% ISM conditions (Fig. 6e, f) result in increases of 161 and 141 kg ha^{-1}. Under each ISM condition the median of the lower elevation distribution either exceeds or is about equal to (Fig. 6a, b) the 66th percentile of the corresponding high elevation distribution. However, this general increase in yields may be due to factors other than the higher GDD totals at lower elevations seen in Fig. 2a and b. Specifically, this positive yield effect might be due in part to the approximately 50 mm higher median summer rainfall seen in the lower elevation station's precipitation percentiles in Fig. 2c.

The modeling approach used here to isolate temperature's effects on simulated lower elevation yields was to adjust the daily weather records of the 22 high elevation stations to simulate the warmer conditions of lower elevations, while preserving the higher elevation precipitation properties. These adjustments, which are described in Appendix A, account for the temperature effects of an adiabatic lapse rate, increasing atmospheric optical depth on surface radiation, and the effect on dew point temperature assuming a constant vapor pressure deficit. The resulting adjusted weather records were then used as inputs to the CSM-CROPGRO-Cotton model to simulate yields that would be produced by the higher elevation station's precipitation patterns, but at lower and warmer elevations. For each ISM-PO condition, this process also produced yields based on adjusted weather inputs for each high elevation station-year, making comparisons with yields based on the unadjusted high elevation weather records possible. The resulting yield effect distributions, in principle, reflect only the temperature effects of elevation.

Fig. 7a, c, and e reproduce the lint yield distributions of Fig. 6a,c, and e derived from the unadjusted high elevation weather records. Fig. 7b, d, and f show the yield percentiles resulting from the same ISM-PO conditions, but generated with high elevation weather records adjusted via Eqs. (A1)–(A8). Thus the latter BW diagrams estimate the distributions of yields resulting from lower elevation temperature and radiative conditions, but with precipitation records identical to those used to generate Fig. 7a, c, and e distributions.

The percentiles of Fig. 7b, d, and f are, with the exception of Fig. 7b's maximum yield value, uniformly shifted to higher yield levels relative to their counterparts in Fig. 7a, c, and e. These distributional shifts supports the position that similar positive shifts in Fig. 6 low altitude yields are mainly due to elevation-related temperature effects. But under the 20% ISM condition Figs. 6f and 7f also show evidence of a low elevation precipitation effect on yield. The extent of Fig. 7f's central tercile shows a 33% chance that a yield outcome under the driest ISM condition will fall with the range 252–502 kg ha^{-1} under the low elevation temperature and high elevation precipitation conditions. But under Fig. 6f's low elevation temperature and low elevation precipitation simulations that central tercile range broadens to 245–600 kg ha^{-1}. This suggests that the somewhat wetter lower

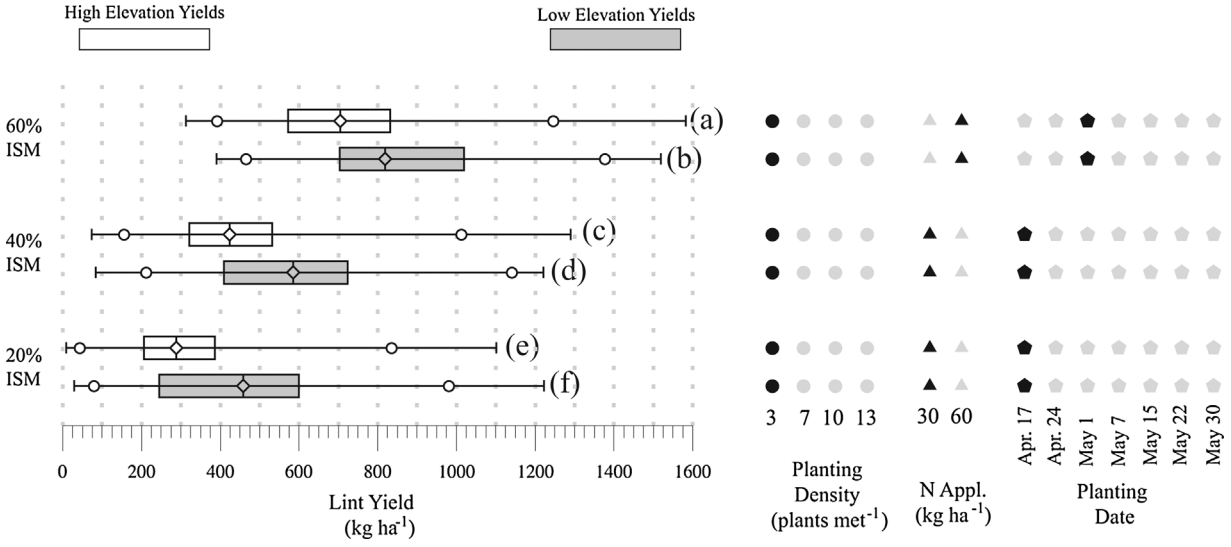

Fig. 6. a) Lint yield percentiles for the planting option producing the highest median yield at high elevation (PO 10) under 60% ISM conditions. b) Lint yield percentiles generated using the same planting option and ISM condition in (a), but with low elevation weather inputs. c) Lint yield percentiles for the planting option producing the highest median yield at high elevation (PO 1) under 40% ISM conditions. d) Percentiles generated using the same planting option and ISM condition in (c), but with low elevation weather inputs. e) Lint yield percentiles for the planting option producing the highest median yield at high elevation (PO 1) under 20% ISM conditions. f) Lint yield percentiles generated using the same planting option and ISM condition in (e), but with low elevation weather inputs.

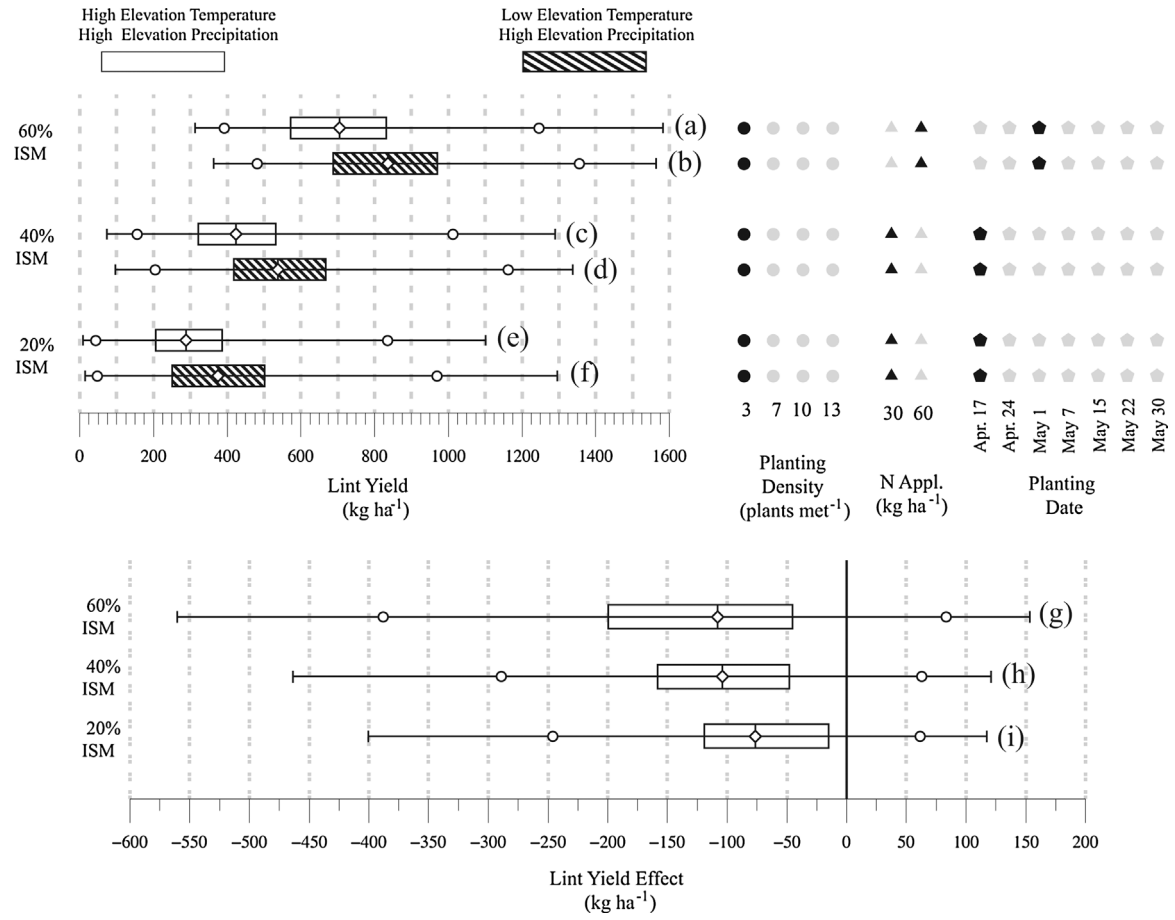

Fig. 7. a) Percentiles of high elevation lint yields for the planting option producing the highest median yield under 60% ISM conditions. b) Lint yield percentiles generated using the same planting option and ISM condition in (a), but with low elevation temperature − high elevation precipitation weather inputs formed via the procedure described in the Appendix A. c) As in (a) for the planting option producing the highest median yield under 40% ISM conditions. d) Lint yield percentiles generated using the same planting option and ISM condition in (c), but with low elevation temperature and high elevation precipitation weather inputs. e) As in (a) for the planting option producing the highest median yield under 20% ISM conditions. f) Lint yield percentiles generated using the same planting option and ISM condition in (e), but with low elevation temperature and high elevation precipitation weather inputs. g) Percentiles of temperature-related yield effects resulting from subtracting the yields of distribution (a) from the same station-year's yield in distribution (b). h) Percentiles of temperature-related yield effects resulting from subtracting the yields of distribution (c) from the same station-year's yield in distribution (d). i) Percentiles of temperature-related yield effects resulting from subtracting the yields of distribution (e) from the same station-year's yield in distribution (f).

elevation conditions indicated in Fig. 2c may be playing a role in generating higher lint yields under Fig. 6f's driest initial soil moisture condition.

Unlike the BW diagrams of Fig. 6a and b, a station-year to station-year correspondence exists between yields within Fig. 7a and b distributions. As a result, yield effect distribution similar to Fig. 5g can be formed. Fig. 7g shows the distribution of Δ_Y that result when Fig. 7b yields are subtracted from the same station-year's yield in Fig. 7a distribution derived from unadjusted high elevation weather records. Given the generally yield decreasing effects on production at cooler high elevation temperatures, Fig. 7g estimates the yield reducing effects of higher elevation conditions under the PO 10 management option for 60% ISM conditions. Similarly, Fig. 7h shows the yield reducing effects of elevation under the optimal option for 40% conditions (i.e., Fig. 7c minus Fig. 7d yields), while Fig. 7i shows the elevation effects on the optimal 20% management option (i.e., Fig. 7e minus Fig. 7f yields).

The magnitudes of the negative median yield effects of higher elevation in Fig. 7g–i ($-76, -104, -108$ kg ha^{-1}) are between 50% to 58% of the positive median yield effects of the optimal planting options in Fig. 5g–i (146, 180, 215 kg ha^{-1}). This suggests that the yield increasing effects of an optimal management strategy may be considerably neutralized by the effects of elevation. From an alternative, more optimistic standpoint, it also suggests that elevation's yield reducing effects may be somewhat compensated for by selecting optimal planting options at higher elevations. Although elevation's yield reducing effects are not exclusively negative ($\Delta_Y < 0$), under each of the ISM conditions in Fig. 7g–i the yield effect distributions show a greater than 78% probability of a negative effect. The 66th percentile of Fig. 7g (–45 kg ha^{-1}) indicates a 66% probability that a negative yield effect will exceed that value under the highest ISM condition. Under the 40% and 20% conditions of Fig. 7h and i, that 66% probability threshold shifts to -48 and -15 kg ha^{-1} respectively.

6. Discussion

The modeled yield effects found here show that the cooler SHP summer season growing conditions reduce median dryland lint yields relative to those at lower elevations. This effect is particularly clear under the 40% and 60% initial soil moisture (ISM) conditions (e.g., Fig. 4a,d). Of the three variables that define the 56 planting options in these simulations − planting density, nitrogen application, and planting date − planting date and density account for the most variability in the SHP region's median yield outcomes. As planting dates are delayed, higher elevation median yields decrease relative to lower elevation yields in Fig. 4c, f, and i, which suggests this effect is a consequence of the lower growing degree day totals accumulated at higher elevation (Fig. 2b). Of course, the planting of cotton on the Southern High Plains is not determined by the calendar, but by soil temperature

(Boman and Lemon, 2005). However, these results suggest that the cooler conditions at higher elevations might be compensated for by extending the duration of the SHP growing season by planting on the earliest date that soil temperatures permit. The planting options that maximize median yields for all three ISM conditions at higher elevations also include low planting densities (Fig. 5a, c, and e), while the highest planting densities produce the smallest median yields (Fig. 5b, d, and f). Combined with the effects of planting date on median yield in Fig. 4, this suggests that the corresponding yield effects of Fig. 5g–i are mainly driven by the choice of planting density and date. As a result, low planting density and earlier planting may be common features of management practices that increase dryland cotton yields and profits over the SHP cotton production region, assuming suitable soil moisture and temperature conditions in the spring.

Having identified best planting options for high elevation production, the distributions of yields resulting from those options under high and low elevation conditions were compared in Fig. 6. Using the weather input adjustment procedure described in the Appendix A, the negative yield effects attributable only to temperature effects, i.e., the cooler production conditions of the SHP, were also estimated (Fig. 7g–i). Fig. 4's clear positive median yield effects at lower elevation, and the percentile effects found in Figs. 6 and 7, shows a Rolling Plains yield advantage in producing un-irrigated upland cotton due to the effects of elevation and temperature. It is emphasized that the modeled yield results presented here are hypothetical, and attributable only to the effects of planting practices and elevation for a fixed soil type. The effects of varying soil types and cultivars, insect or disease pressure, and the actual distribution of initial soil moisture conditions are not considered. However, by controlling for these non-climatic production factors these simulations indicate a lower elevation production advantage related to climate. As a result, although in the past the Southern High Plains has been the leading West Texas cotton production region due to the irrigation resource of the Ogallala Aquifer, these results further suggest the possibility of dryland production migrating to the Rolling Plains region as the aquifer depletes.

A common feature in Figs. 5–7 are bar and whisker diagrams representing yield and yield effect distributions. These distributions were used here to estimate the probability of yield outcomes under selected planting option and initial soil moisture conditions. Those probabilities can in turn be interpreted in terms of the current yield risk associated with those conditions. Although the WTM weather records used here are shorter than the 30 year periods normally used to define climate (Guttman 1989; WMO 1989), Livezey et al. (2007) contend that under changing climate conditions 30 year normals are frequently unrepresentative of current climate. Trewin (2007) has proposed the use of operational climate normals that might be formed from as little as ten years of recent data. The approach demonstrated here used the WTM's dense network of weather stations to form similarly dense distributions of yield outcomes during 2005–2015, thus these results may be considered representative of the current climate of the SHP and Rolling Plains regions. Over other growing areas where mesonet data is unavailable, a similar modeling and aggregation approach might be based on weather inputs from stochastic weather generators (Wilks 2010, 2012). The translation of yield outcomes into profits under current or projected price and cost conditions would result in corresponding profit distributions that estimate a producer's current economic risk. This general simulation and aggregation process may be, in the absence of skillful seasonal forecast information, the best available approach to estimating production risk related to the essentially unpredictable year-to-year variation in growing season climate.

Acknowledgements

The authors would like to thank NOAA's National Mesonet Project and Texas Tech University for continued support in maintaining the West Texas Mesonet. Thanks to Kendall DeJonge for helpful advice regarding crop model calibration. All figures were produced using Generic Mapping Tools (Wessel and Smith, 1995). This research did not receive any specific grant from funding agencies in the public, commercial, or not-for-profit sectors. The USDA is an equal opportunity provider and employer.

Appendix A

To form adjusted CSM-CROPGRO-Cotton weather input files for each of the 22 high elevation stations during the 10 simulation years, the station's daily values of T_{min}, T_{max}, T_{dew}, and R_S were adjusted to values that assumed an elevation drop equal to the mean difference in elevation between Fig. 1's high and low elevation stations ($\Delta Z = -410$ met.). The adjusted daily T_{min} (T'_{min}) and T_{max} (T'_{max}) values were calculated using an atmospheric lapse rate equal to that of the International Standard Atmosphere ($\gamma = -0.0065\ ^{\circ}C\ m^{-1}$).

$$T'_{min} = T'_{min} + \gamma^{*}\Delta Z \quad \text{(A1a)}$$

$$T'_{max} = T'_{max} + \gamma^{*}\Delta Z \quad \text{(A1b)}$$

As increasing atmospheric optical depth can have an attenuating effect on short-wave surface radiation, adjusted R_S values (R'_S) were calculated based on Allen et al.'s (1998) formula (their Eq. 3-13) for estimating clear sky solar radiation as a function of elevation. With $Z' = Z + \Delta Z = Z - 410$ m, the adjusted daily surface solar radiation values were estimated from the unadjusted WTM R_S values and the station's actual and adjusted elevations via,

$$R'_S = R_S{}^{*}\frac{0.75 - 2{*}10^{-5}{*}Z'}{0.75 - 2{*}10^{-5}{*}Z} \quad \text{(A2)}$$

Given the role of dew point temperature in calculating the vapor pressure deficit (VPD) values used in CSM-CROPGRO-Cotton's evapotranspiration calculations (Eq. (2)), adjusted dew point temperatures (T'_{dew}) were estimated based on the assumption that adjusted (VPD'),

$$VPD' = e'_s - e'_a \quad \text{(A3a)}$$

and unadjusted vapor pressure deficit,

$$VPD = e_s - e_a \quad \text{(A3b)}$$

are equal. Vapor pressure (e_a) and saturation vapor pressure (e_s) were calculated via the Clausius-Clapeyron equation of Allen et al. (1998), where,

$$e_a = e(T_{dew}) \quad \text{(A4a)}$$

$$e'_a = e(T'_{dew}) \quad \text{(A4b)}$$

Saturation vapor pressures are estimated using the daily adjusted and unadjusted T_{min} and T_{max} values,

$$e'_s = 0.5*(e(T'_{max}) + e(T'_{min})) \quad (A5a)$$

$$e_s = 0.5*(e(T_{max}) + e(T_{min})) \quad (A5b)$$

Thus under constant VPD can be calculated given the unadjusted T_{max}, T_{min}, and T_{dew} values, and the lapse rate adjusted and T'_{min} values of Eqs. (A1a) and (A1b),

$$e'_a = e_a - e_s + e'_s \quad (A6)$$

The adjusted T'_{dew} value can then be solved for by inverting the Clausius-Clapeyron equation,

$$T'_{dew} = \frac{\beta*273.3}{17.27 - \beta} \quad (A7)$$

where,

$$\beta = \ln\left(\frac{e'_a}{0.6108}\right) \quad (A8)$$

The remaining two CROPGRO-Cotton daily weather input variables, daily precipitation and wind run, were unchanged from their observed WTM values in the adjusted high elevation weather data files.

References

Adhikari, P., Ale, S., Bordovsky, J.P., Thorp, K.R., Modala, N.R., Rajan, N., Barnes, E.M., 2016. Simulating future climate change impacts on seed cotton yield in the Texas High Plains using the CSM-CROPGRO-Cotton model. Agric. Water Manage. 164, 317–330.

Allen, R.G., Pereira, L.S., Raes, D., Smith, M., 1998. Crop Evapotranspiration: Guidelines for Computing Crop Water Requirements. FAO Irrig. and Drain. Paper No. 56. Food and Agriculture Organization of the United Nations 300 pp.

Angulo, C., Rötter, R., Lock, R., Enders, A., Fronzek, S., Ewert, F., 2013. Implication of crop model calibration strategies for assessing regional impacts of climate change in Europe. Agric. Forest Meteor. 170, 32–46.

Baumhardt, R.L., Staggenborg, S.A., Gowda, P.H., Colaizzi, P.D., Howell, T.A., 2008. Modeling irrigation management strategies to maximize cotton lint yield and water use efficiency. Agron. J. 101, 460–468.

Boman, R. and R., Lemon, 2005. Soil Temperatures for Cotton Planting. Texas A & M AgriLife Extention SCS-2005-17. Retrieved Aug. 19 2016 from http://cotton.tamu.edu/General%20Production/scs-2005-17%20Soil%20Temp.pdf.

Boote, K.J., Sau, F., Hoogenboom, G., Jones, J.W., 2008. Experience with water balance, evapotranspiration, and predictions of water stress effects in the CROPGRO model. In: Reddy, V.R., Ahuja, L.R., Sassendran, S.A., Yu, Q. (Eds.), Response of Crops to Limited Water: Understanding and Modelling Water Stress Effects on Plant Growth Processes. ASA – CSSA – SSSA, pp. 59–103.

Bordovsky, J., and J., Mustian, 2013. Evaluation of Zero-early Cotton Irrigation Strategy. In: Helm Research Farm Summary Report 2013 (Technical Report No. 14-4). Texas A & M Agrilife Research. Retrieved Aug. 18 2016 from http://lubbock.tamu.edu/files/2014/04/Binder1.pdf.

DeJonge, K.C., Thorp, K.R., 2017. Standardized Reference Evapotranspiration and Dual Crop Coefficient Approach in the DSSAT Cropping System Model. Trans. ASABE (In review).

DeJonge, K.C., Ascough Ii, J.C., Ahmadi, M., Andales, A.A., Arabi, M., 2012a. Global sensitivity and uncertainty analysis of a dynamic agroecosystem model under different irrigation treatments. Ecol. Model. 231, 113–125.

DeJonge, K.C., Ascough II, J.C., Andales, A.A., Hansen, N.C., Garcia, L.A., Arabi, M., 2012b. Improving evapotranspiration simulations in the CERES-Maize model under limited irrigation. Agr. Water Manage. 115, 92–103.

Durre, I., Menne, M.J., Gleason, B.E., Houston, T.G., Vose, R.S., 2010. Comprehensive automated quality assurance of daily surface observations. J. Appl. Meteor. Climatol. 49, 1615–1633.

ERS (USDA Economic Reporting Service), 2016. Cotton and Wool Yearbook. Retrieved Aug. 19 2016 from http://www.ers.usda.gov/data-products/cotton-wool-and-textile-data/cotton-and-wool-yearbook/.

ERS (USDA Economic Reporting Service), 2016. Commodity Costs and Returns.Retrieved Aug. 19 2016 from https://www.ers.usda.gov/data-products/commodity-costs-and-returns/commodity-costs-and-returns/#Recent%20Costs%20and%20Returns:%20Cotton.

Elizondo, D., Hoogenboom, G., McClendon, R.W., 1994. Development of a neural network model to predict daily solar radiation. Agric. For. Meteorol. 71, 115–132.

Guttman, N.B., 1989. Statistical descriptors of climate. Bull. Amer. Meteorol. Soc. 70, 602–607.

Haacker, E.M.K., Kendall, A.D., Hyndman, D.W., 2016. Water level declines in the High Plains Aquifer: predevelopment to resource senescence. Groundwater 54, 231–242. http://dx.doi.org/10.1111/gwat.12350.

Hanson, C.L., Cummings, A., Woolhiser, D.A., Richardson, C.W., 1994. Microcomputer Program for Daily Weather Simulation in the Contiguous United States. ARS 114. National Technical Information Service, Alexandria, VA.

Hillel, D., Rosenzweig, C., 2011. Handbook of Climate Change and Agroecosystems: Impacts, Adaptation, and Mitigation, vol. 1 Imperial College Press (440 pp.).

Hoerling, M., et al., 2013. Anatomy of an extreme event. J. Climate 26, 2811–2832.

Hoogenboom, G., Jones, J.W., Wilkens, P.W., Porter, C.H., Boote, K.J., Hunt, L.A., Singh, U., Lizaso, J.L., White, J.W., Uryasev, O., Royce, F.S., Ogoshi, R., Gijsman, A.J., Tsuji, G.Y., Koo, J., 2012. Decision Support System for Agrotechnology Transfer (DSSAT). University of Hawaii, Honolulu, Hawaii (Version 4.5.1.005).

Hosking, J.R.M., Wallis, J.R., 1997. Regional Frequency Analysis: An approach based on L moments? Cambridge University Press (224 pp.).

Howell, T.A., Evett, S.R., Tolk, J., Schneider, A., 2004. Evapotranspiration of full-, deficit-irrigated, and dryland cotton on the northern Texas high plains. J. Irrig. Drain E-ASCE 130, 277–285.

Jones, J.W., et al., 2003. The DSSAT cropping system model. Eur. J. of Agron. 18, 235–265.

Livezey, R.E., Vinnikov, K.Y., Timofeyeva, M.M., Tinker, R., van den Dool, Huug M., 2007. Estimation and extrapolation of climate normals and climate trends. J. Appl. Meteorol. Climatol. 46, 1759–1776.

Mauget, S., Zhang, J., Ko, J., 2009. The value of ENSO forecast information to dual-Purpose winter wheat production in the U.S. southern high plains. J. Appl. Meteorol. Climatol. 48, 2100–2117.

Mauget, S., Leiker, G., Nair, S., 2013. A web application for cotton irrigation management on the U.S: Southern High Plains. Part I: Crop yield modeling and profit analysis. Comput. Electron. Agric. 99, 248–257.

McGuire, V.L., 2007. Changes in water levels and storage in the high plains aquifer, predevelopment to 2005 and 2003–2005. Geol. Surv. Scientific Invest. Rep. 2006–5324, 7.

Messina, C., Ramkrishnan, J.W., Jones, K.J., Boote, G., Hoogenboom, J.T., 2004. A simulation model of cotton growth and development for CSM. In: Proc. Biological Systems Simulation Group (BSSG) Conference. Gainesville, FL, University of Florida. pp. 54–55.

Morrow, M.R., Krieg, D.R., 1990. Cotton management strategies for a short growing season environment: water-nitrogen considerations. Agron. J. 82, 52–56.

NASS (USDA National Agricultural Statistical Service), 2016. Quickstats 2.0. 2012 Agricultural Census. Retrieved Aug. 17 2016 from https://quickstats.nass.usda.gov/?source_desc=CENSUS.

NASS (USDA National Agricultural Statistical Service), 2016. Quickstats 2.0.Retrieved Aug. 17 2016 from. https://www.nass.usda.gov/Quick_Stats/Ag_Overview/stateOverview.php?state=texas.

NASS (USDA National Agricultural Statistical Service). 2016. Quickstats 2.0. Retrieved Oct 4 2016 from https://quickstats.nass.usda.gov.

Pathak, T.B., Jones, J.W., Fraisse, C.W., Wright, D., Hoogenboom, G., 2012. Uncertainty analysis and parameter estimation for the CSM-CROPGRO-Cotton model. Agron. J. 104, 1363–1373.

Pathak, T.B., Fraisse, C.W., Jones, J.W., Messina, C.D., Hoogenboom, G., 2007. Use of global sensitivity analysis for CROPGRO cotton model development. Trans. ASABE 50, 2295–2302.

Peng, S., Krieg, D.R., Hicks, S.K., 1989. Cotton lint yield response to accumulated heat units and soil water supply. Field Crop. Res. 19, 253–262.

Reddy, K.R., Kakani, V.G., Hodges, H.F., 2008. Exploring the use of the environmental productivity index concept for crop production and modeling. In: Ahuja, L.R., Reddy, V.R., Sassendran, S.A., Yu, Q. (Eds.), Response of Crops to Limited Water: Understanding and Modeling Water Stress Effects on Plant Growth Processes. ASA-SSSA-CSSA, pp. 387–410.

Rosenzweig, C., Hillel, D., 1993. Agriculture in a greenhouse world. Natl. Geogr. Res. and Explor. 9, 208–221.

Scanlon, B.R., Faunt, C.F., Longuevergne, L., Reedy, R.C., Alley, W.M., McGuire, V.L., McMahon, P.B., 2012. Groundwater depletion and sustainability of irrigation in the US High Plains and Central Valley. Proc. Natl. Acad. Sci. U. S. A. 109, 9320–9325.

Schroeder, J.L., Burgett, W.S., Haynie, K.B., Sonmez, I., Skwira, G.D., Doggett, A.L., Lipe, J.W., 2005. The west Texas Mesonet: a technical overview. J. Atmos. Ocean. Technol. 22, 211–222.

Soler, C.M., Hoogenboom, G., 2006. Simulating cotton growth and development under different irrigation scheduling regimes. In: Abstracts of the ASA-SSSA-CSSA Intl. Annual Meeting. Madison, Wisc.: ASA-SSSA-CSSA.

Sophocleous, M., 2010. Review: groundwater management practices, challenges, and

innovations in the High Plains aquifer: USA—lessons and recommended actions. Hydrogeol. J. 18, 559–575.
Stapper, J.R., Fromme, J.R., 2011. Comparative Growth and Yield of Cotton at Various Planting Densities (Lawhon Farm Study). Texas A & M AgriLife Extention Service. http://nueces.agrilife.org/files/2011/08/Lawhon-plant-pop-study.pdf.
Thorp, K.R., Barnes, E.M., Hunsaker, D.J., Kimball, B.A., White, J.W., Nazareth, V.J., Hoogenboom, G., 2014. Evaluation of CSM-CROPGRO-COTTON for simulating effects of management and climate change on cotton growth and evapotranspiration in an arid environment. T. ASABE 57, 627–1642.
Tolk, J.A., Howell, T.A., 2010. Cotton water use and lint yield in four Great Plains soils. Agron. J. 102, 904–910.
The role of climatological normals in a changing climate., World Climate Data and Monitoring Program No. 61, WMO-TD No. 1377, 46 pp.
USGS (U.S. Geological Survey) 2015: Global 30 arc second elevation (GTOPO30). Retrieved Mar. 22 2007 from https://lta.cr.usgs.gov/get_data.
Walter, I.A., et al., 2005. The ASCE Standardized Reference Evapotranspiration Equation. Final Report on the Tech Committee on Standardization of Reference Evapotranspiration. ASCE Environmental and Water Resources Institute, Reston VA. http://www.kimberly.uidaho.edu/water/asceewri/ascestzdetmain2005. pdf.
Wessel, P., Smith, W.H.F., 1995. New version of the generic mapping tools. Eos Trans. Amer. Geophys. Union 76, 329.
Wilks, D.S., 2010. Use of stochastic weather generators for precipitation downscaling. Wiley Interdiscip. Rev. Clim. Change 1, 898–907.
Wilks, D.S., 2012. Projecting normals in a nonstationary climate. J. Appl. Meteorol. Climatol. 52, 289–302.
WMO (World Meteorological Organization). 1989. Calculation of monthly and annual 30-year standard normals. WMO-TD No. 341, 12 pp.].